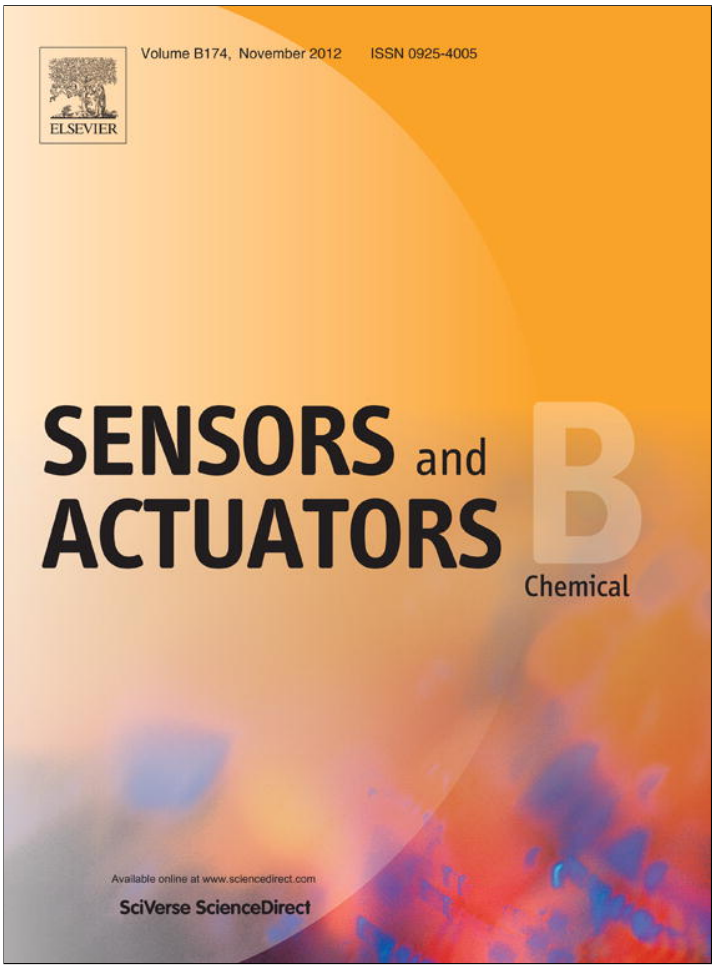

Sensors and Actuators B 174 (2012) 609–615

Contents lists available at SciVerse ScienceDirect

Sensors and Actuators B: Chemical

journal homepage: www.elsevier.com/locate/snb

Fluorescent magnetic bead and cell differentiation/counting using a CMOS SPAD matrix

Emile P. Dupont[a], Estelle Labonne[b,1], Yuki Maruyama[c], Caroline Vandevyver[d], Ulrike Lehmann[a,2], Martin A.M. Gijs[a], Edoardo Charbon[b,c,*]

[a] Laboratory of Microsystems, Ecole Polytechnique Fédérale de Lausanne (EPFL), CH-1015 Lausanne, Switzerland
[b] School of Engineering, Ecole Polytechnique Fédérale de Lausanne (EPFL), CH-1015 Lausanne, Switzerland
[c] Circuits and Systems Group, Faculty of EEMCS, Delft University of Technology, Delft, The Netherlands
[d] Research Commission EPFL-SNF, Ecole Polytechnique Fédérale de Lausanne (EPFL), CH-1015 Lausanne, Switzerland

ARTICLE INFO

Article history:
Received 28 October 2011
Received in revised form 7 May 2012
Accepted 23 June 2012
Available online 14 July 2012

Keywords:
Immunofluorescence
Microfluidics
Single photon avalanche diode
Integrated CMOS chip
MCF-7
Single cell detection

ABSTRACT

We present a monolithic silicon chip comprising a matrix of 84 single photon avalanche diodes (SPADs) to detect and discriminate fluorescent beads or fluorescently labeled single cells in a polydimethyl(-siloxane) (PDMS) cartridge that is positioned on top of the chip. Our detection is based on the different photon count when either a fluorescent or non-fluorescent bead or cell is present above a SPAD, due to the additional photons emitted from a fluorescent object. Our technique allows microscope-less fluorescence detection and permits easy exchange of the disposable microfluidic cartridge. We first demonstrate the working principle of our device by counting and discriminating fluorescent from non-fluorescent 3, 6 and 10 μm magnetic beads, which are commonly used as versatile mobile carriers for separating a target analyte from a matrix via magnetic forces in microfluidic lab-on-a-chip systems. We then apply our system to count and discriminate fluorescently-labeled MCF-7 breast cancer cells from unlabeled Jurkat cells mixed in a phosphate buffer saline (PBS) solution. Our device is robust and does not need complex microfluidic handling to achieve cell count without the need of external fluorescence detection bulky equipment.

1. Introduction

Lab-on-chip systems in recent times have increasingly used magnetic micro- and nanoparticles (beads) for bio-analytical and diagnostic applications; this success is due to the intrinsic compatibility of the beads size with the microfluidic format. This enables accurate bead discrimination, counting or quantitative immunofluorescent detection, instead of analyzing the average signal from a larger populations of particles [1]. Cell identification and counting is another important area of research, whereas a small liquid sample (blood, saliva) can be a crucial disease indicator and can help in patient's diagnosis. For example, the presence of tumor cells in blood is a signal of metastasis, and the concentration of these cells is an indicator for either healing or relapse following chemotherapy [2], and the concentration of a particular white blood cell line (CD4+) in blood is correlated with the progression of HIV infection [3–6].

Fluorescence-activated cell sorting (FACS) and magnetic activated cell sorting (MACS) methods are commonly used in a conventional laboratory environment [7–9,36,40,49]. FACS analysis is the gold standard of high-throughput cell counting, in which the cells are discriminated based on their immunofluorescence [10,11]. However, flow cytometers and FACS systems are complex instruments that rely on focusing of the cells in a narrow stream and require the use of bulky and expensive fluorescence microscope setups. Thus, there is currently much interest for portable and easy-to-use cell counting based on microfluidics. While manual or semi-automatic counting chambers can be used for cell concentration and characterization of cell cultures, these techniques suffer from the possibility of operator's and/or statistical errors. Most importantly, external hardware and high end microscopic setups are still essential for successful implementation of these methods [12–16]. Several advantages are offered by a microfluidic system, namely, low reagent consumption (typically a few μLs), the possibility to mass-produce and to integrate several analysis modules enabling portable automated applications, fast analysis and low cost.

In recent years, lab-on-a-chip systems have been increasingly developed for systems biology and cell-based assays, due to the

* Corresponding author at: Delft University of Technology, Mekelweg 4, 2628 CD Delft, The Netherlands.
E-mail address: e.charbon@tudelft.nl (E. Charbon).
[1] Current address: CEA-LETI, 38054 Grenoble, France.
[2] Current address: Microsens SA, 2002 Neuchâtel, Switzerland.

0925-4005/$ – see front matter © 2012 Elsevier B.V. All rights reserved.
http://dx.doi.org/10.1016/j.snb.2012.06.049

intrinsic compatibility of cell size with the microsystem format [39,43,45,50]. This area of research, also known as cellomics, has been reviewed extensively [1,17,18]. Fu et al. proposed a microfluidic device for fluorescent cell sorting. The sorting mechanism was based on fluorescence detection using an inverted microscope setup [19]. Jokerst et al. presented a system comprising a capture membrane to filter specifically a CD4+ cell population and used quantum dots as fluorescent antibody(Ab)-conjugated markers on the cells [20]. Cheng et al. proposed the use of a device comprising the detection of specifically captured cells on a functionalized surface using an impedance measurement directly integrated on-chip [21], but such approach, in contrast to systems that operate under continuous flow conditions, can suffer from saturation of the sensor when a high number of cells are captured, or from non-specific cell adsorption and binding on the surface. Using impedimetric detection, Jiang et al. presented a microchip for the precise counting of cells [22], focusing on improving the limit of detection (LOD). The group of Ozcan recently presented a lensfree microscopy system to image fluorescent and non-fluorescent cells [23–25]. The same group also published lens-free fluorescent imaging on a chip [26,27]. In this paper, we propose the use of a single-photon avalanche diode (SPAD) matrix integrated in CMOS for the direct counting of magnetic beads and cells in a PDMS microfluidic cartridge without the need of a microscope setup. Our device is small, portable, reusable and does not require additional emission filters or mirrors for the fluorescent signal detection. A further advantage of this setup is that no additional image processing or manipulation softwares are required for the count. A SPAD is a reverse-biased p–n junction biased above breakdown, in so-called Geiger mode of operation, capable to detect single photons incident on its active area. In our experimental protocol, the sample we analyze is flown within a disposable PDMS microfluidic cartridge positioned on top of the SPAD matrix. The detection and recognition of fluorescently-labeled particles and cells is achieved on-chip, by counting the photons hitting each single SPAD of the matrix. Thanks to the high sensitivity of SPADs in the wavelength of emission, it is possible to perform quick and accurate analysis while background illumination and noise are accounted and compensated for.

2. Materials and methods

2.1. Materials

A phosphate buffer saline (PBS) (0.15 M, pH = 7.4) was prepared by dissolving PBS powder (product no. P3813) in deionized (DI) water. PBS–bovine serum albumin (PBS–BSA) at different concentrations was prepared by dissolving PBS–BSA powder (product no. P3688) in DI water. For hydrophilisation of the microfluidic channel, 100 mL of 0.25% solution of polyvinylpyrrolidone (PVP) were prepared by dissolving PVP powder in DI water (product no. 234257). All these chemicals were obtained from Sigma Aldrich (Buchs, Switzerland). 3, 6 and 10 μm diameter non-functionalized fluorescent microspheres (product no. UMC3F-3 μm, UMC3F-6 μm and FS06F, respectively) were purchased from Bangs Laboratories (Fischer, IN, USA), as well as non-fluorescent 3, 6 and 10 μm diameter beads (product no. UMC3F, PMS3N and BM547 respectively). 5D10 monoclonal antibody (mAb) was obtained from the University of Hasselt, Biomedical Research Institute, Diepenbeek, Belgium, and labeled with Alexa Fluor® 647 from Invitrogen (Basel, Switzerland, product no. A20173), and prepared according to the manufacturer's instructions.

2.2. Microfluidic cartridge fabrication

Sylgard 184 polydimethylsiloxane (PDMS) was purchased from Dow Corning (Midland, USA). We prepared the microfluidic cartridge body and membrane with a standard 10:1 PDMS base-to-catalyst ratio. We used a master mold for fabricating the cartridge body composed of two separate parts: a 35 μm high, 200 μm wide and 5 cm long SU8 microchannel structure realized on a silicon substrate by standard clean room fabrication techniques, combined with a macroscopic poly(methyl-methacrylate) (PMMA) part, to form the bigger millimeter-size features used for the integration and the alignment of the cartridge over the motherboard. After demolding of the microfluidic cartridge body, a microchannel sealing membrane is fabricated by spinning liquid PDMS on a Pyrex wafer (Guinchard Optical Glass, Yverdon-les-Bains, Switzerland) at 3500 rpm for 40 s on a spin coater (Delta 20 BM by B.L.E. Laboratory Equipment GmbH, Radolfzell, Germany), to obtain a PDMS membrane thickness of 20 μm. The PDMS cartridge body and the membrane are then irreversibly sealed together by exposing both sides to be bonded to an air plasma treatment at 20 W for 30 s, with the membrane still on the Pyrex wafer. The completed bonded cartridge can then be simply mechanically stripped-off from the wafer. The plasma treatment also increases the surface energy of the microchannel's walls, but only for a short period of time; for easy filling of the PDMS microchannel, we apply and incubate for 12 h a hydrophilizing polyvinylpyrrolidone (PVP) solution within the cartridge. Hereafter the microchannel is rinsed with DI water.

2.3. Cell culture

The human breast adenocarcinoma cell line MCF-7 (ATCC HTB-22) and human leukemia cell line Jurkat (ATCC TIB 152) were cultivated in 75 cm^2 culture flasks using RPMI 1640 (Sigma, R8758) supplemented with 5% fetal calf serum (FCS), 2 mM L-glutamine, 1 mM sodium pyruvate, 1% non-essential amino-acids, 1% 4-(2-hydroxyethyl)-monosodium salt (HEPES) (all from Gibco® Cell Culture, Invitrogen). Cultures were maintained at 37 °C under 5% CO_2. The growth medium was changed every other day until the time of use of the cells. Cell density and viability, defined as the ratio of the number of viable cells over the total number of cells, of the cultures were determined using trypan blue staining and a Neubauer improved haemocytometer (Blau Brand, Wertheim, Germany).

2.4. Cell fixation and immunofluorescent staining

MCF-7 cells were detached and harvested with trypsin–EDTA solution (Sigma T4049, Switzerland) when the cells were confluent. The detached cell suspensions were centrifuged at 250 × *g* for 5 min and cells were washed with 5 ml PBS (3×). The cell pellets were resuspended in 1% paraformaldehyde solution (0.5% BSA–PBS) on ice for 5 min. The cells were centrifuged three times with 0.5% BSA/PBS at 250 × *g* for 5 min. Ice-cold 100% methanol was added drop-wise with constant agitation and cell suspensions were then centrifuged three times at 250 × *g* for 5 min. Jurkat cells were fixed using the same protocol. The fixed MCF-7 cells were incubated with 1 ml of 10 μg/mL fluorescent 5D10 mAb for 30 min at 4 °C, washed and centrifuged four times with 1 ml of 0.5% PBS–BSA. The fluorescent MCF-7 cells were incubated with 0.4% glutaraldehyde for 10 min at 4 °C, and then washed and centrifuged four times with 1 mL of 0.5% PBS–BSA.

2.5. SPAD matrix chip design and setup

The chip was fabricated on 0.35 μm HV CMOS process, where SPADs are based on a circular design with a guard ring to prevent premature edge breakdown [28]. Fig. 1(a) shows a cross-sectional view of the SPAD matrix realized with the equivalent electrical circuit for quenching and readout. Fig. 1(b) is a micrograph of the SPADs arrangement as seen from the top, while the inset shows a

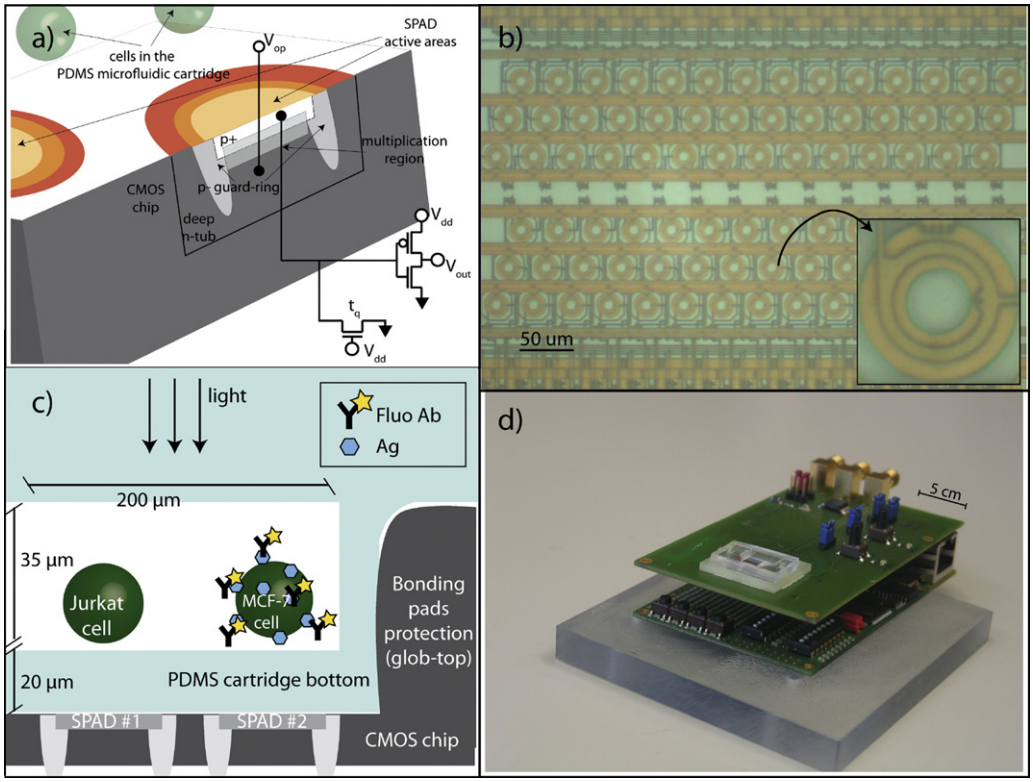

Fig. 1. (a) Oblique schematic representation of a SPAD detector with indication of the electrical readout scheme. (b) Optical micrograph of the matrix arrangement of 84 SPADs. The inset is a 5× zoom on one SPAD. (c) Cross-sectional schematic view of the microfluidic cartridge on top of the CMOS chip, and representation of the fluorescent detection principle. Two situations are depicted: a non-fluorescent Jurkat cell and a fluorescently labeled MCF-7 cell positioned over two different SPADs. The dimensions of the microfluidic channel (35 µm × 200 µm) and of the bottom wall thickness (20 µm) are indicated. (d) Microfluidic cartridge positioned on top of a CMOS chip that is bonded onto the daughterboard–motherboard complex.

magnification of one of the SPADs. The SPADs have a circular detection area of 8 µm diameter and their implementation includes 84 SPADs are arranged in a 6 × 14 matrix.

Each SPAD output drives a digital counter through a digital readout circuitry. The distinct features of a SPAD are its virtual lack of readout noise, its extreme dynamic range (over 120 dB), and the achievable time-resolution (in the range of 50–150 ps). The complexity of our SPADs photon detectors was kept intentionally low: the counters used in this chip ensure a very high dynamic range with as low as possible readout frequency, thus minimizing any possible electrical and optical interference coming from complex readout circuitry. Moreover, while designing the chip, we paid attention to the power consumption that we minimized in view of the application. We also achieved due to the matrix arrangement a reduction of the effective pitch to 8.25 µm, which is, to the best of our knowledge, the smallest pitch ever achieved in a SPAD array in this technology. Fig. 2 represents a typical output response of the 84 SPADs to ambient light (light gray bars) versus the dark-count-rate of the same SPADs (black bars). The dark-count-rate of a detector is the response of the device in absence of illumination, and is mainly caused by thermally or tunneling generated carriers within the p–n junction. The figure shows the count values among the different SPADs of the matrix under uniform light exposure. The small variations in the photon count from the SPADs under uniform light are intrinsic noise, caused by different mechanisms [28]. In our setup, possible non-uniformity of the photon count is compensated by the differential measurement with respect to the reference signal of each individual SPAD discussed in the following. The chip's polyimide passivation layer was removed to enhance the photon count and to decrease the distance between the particles inside the microchannel and the SPADs. The chip was bonded with gold wires onto a printed circuit board (PCB) by Hybrid SA, Combamare, Suisse. The custom-made PCB forms an easily exchangeable unit that can be controlled by an in-house designed motherboard and custom-programmed in VHDL language.

For liquid actuation, the bead solution is pushed in the microchannel and the pressure and speed of the flow is controlled using a syringe pump connected to the inlet (neMESYS Cetoni, Korbussen, Germany). Fig. 1(c) is a cross-sectional schematic view of the PDMS cartridge on top of the CMOS chip, with indication of the microchannel dimensions. For the fluorescence experiments, we use a calibrated fluorescent excitation source from a Zeiss microscope (Zeiss Axio Imager.A1m with Hal 100 light-source). An

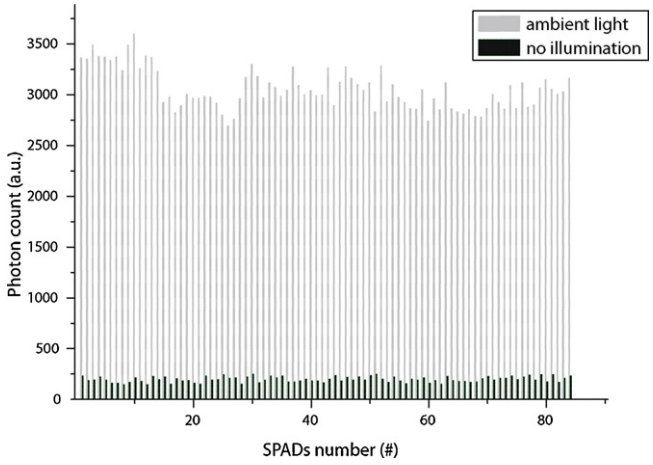

Fig. 2. Photon count for the SPAD matrix under uniform illumination with ambient light, and comparison with the dark count rate (photon count without illumination).

excitation filter (λ_1 = 550 nm, bandpass = 25 nm, from filter set no. 43HE of Zeiss) is placed in between the light source and the CMOS chip–cartridge assembly. Fluorescence images of the cells and the beads in the microchannel are obtained using the same Zeiss microscope with 20× objective and equipped with a Hamamatsu camera (ORCA ER). For comparing optical and fluorescent results, images were recorded without and with an emission filter (λ_2 = 605 nm, bandpass = 70 nm, from filter set no. 43HE of Zeiss), enabling the discrimination of the fluorescent emission of the Alexa 647 dye from the fluorescent excitation signal.

3. Experimental results and discussion

3.1. Measurement protocol

We first filled the PVP-cured PDMS microchannel with PBS–BSA solution, and recorded the SPADs photon count without cells or beads in the channel, providing for each individual SPAD a reference value, allowing the calculation of the differential photon count upon the presence of a fluorescent or non-fluorescent object above the SPAD. Then, a solution of beads or cells was introduced in the channel by means of an external pump. A flow and stop protocol was used, consisting in applying a short flow pulse (~500 ms with a flow rate of 60 nl/min, corresponding to a mean flow velocity of 140 μm/s) followed by a short stop (2 s), during which the cells or beads sediment to the bottom of the microfluidic cartridge and the SPADs are readout. When a bead or cell is present above the SPAD, the output of the latter was recorded. Due to the use of the SPAD matrix, covering the whole lateral cross-section of the microchannel rather than a single detector, no flow focusing is required, and our design intrinsically allows parallel detection.

3.2. Calibration of the device

In order to calibrate the device response with respect to different bead sizes, we tested fluorescent and non-fluorescent beads with diameters ranging from 3 to 10 μm. The differential photon count, defined as the count when a bead is present minus the photon count when the SPAD is fully exposed to light, is dependent on the shadow of the particle blocking the microscope light and thus is larger for larger beads. The relative decrease in light intensity perceived by the SPAD is dependent on the ratio between the radius r_* of the area of view at the bottom of the microfluidic channel, where the particles are present, and the obstacle radius r, following the photometry equation (see Fig. 3) [29,30]:

$$\frac{\Delta I}{I_0} = \left(\frac{r}{r_*}\right)^2 \quad (1)$$

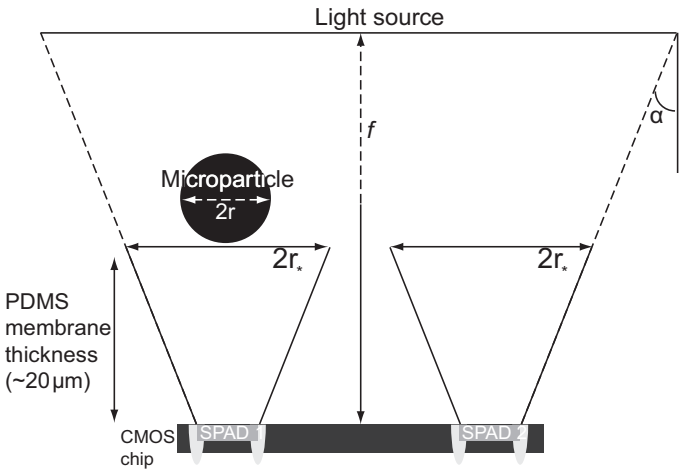

Fig. 3. Schematic of the shadow-based bead detection principle. The light source is a microscope objective with focal distance f = 12 mm and numerical aperture NA = 0.4 corresponding to α = 24°. The radius of r_* the area of view at the bottom of the PDMS microfluidic cartridge, where the bead of radius r is situated during the measurement, is equal to 15 μm.

with

$$r_* = (f + \mathrm{dist_{SPAD}})\tan(\alpha)\frac{r + \mathrm{dist_{SPAD}}}{f} + r_{\mathrm{SPAD}}.$$

The parameters of the light source (in our case, the microscope objective) in Eq. (1) are the focal length f = 12 mm and the angle α = 24°, corresponding to the numerical aperture NA = n sin(α) = 0.4, where we considered a refractive index of n = 1 for air. $\mathrm{dist_{SPAD}}$ = 20 μm is the distance between the bottom of the PDMS channel and the SPAD, and r_{SPAD} = 4.2 μm is the radius of the SPAD. The ratio between the area seen by the SPAD (with a diameter $2r_* \cong 30$ μm) and the biggest observed particle (diameter $2r$ = 10 μm) is around 9, which is of the same order of magnitude as the experimental decrease in photon count perceived by the SPAD.

To verify the dependence of SPAD response on particle size, we tested the system output during observation of non-fluorescent and fluorescent 3, 6 and 10 μm diameter beads. The corresponding normalized differential photon counts are shown in Fig. 4(a). The solid black line shows that the experiment results follow the photometry theory explained before (Eq. (1)). The photon count for fluorescent beads is lower, because of the additional fluorescent photons. The solid gray line fits the data obtained for fluorescently labeled particles, and corresponds to Eq. (1) shifted by 3 μm on the x-axis. Indeed, fluorescent beads with diameters of 3 μm are virtually indistinguishable by the SPADs, because the additional

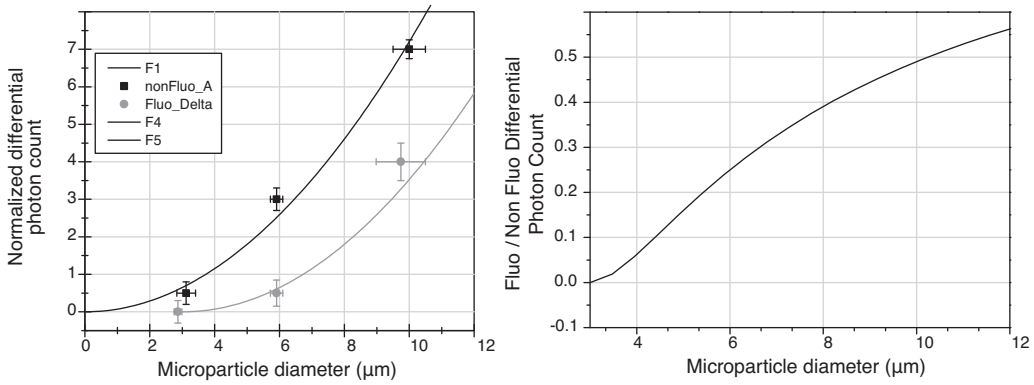

Fig. 4. (a) Comparison of the measured and the theoretical values (Eq. (1)) for non-fluorescent beads of 3, 6 and 10 μm diameter. The response for the fluorescent particles with approximately the same dimensions (gray circles) is lower, due to the additional fluorescent photons. (b) Ratio between the normalized differential photon count of the SPAD during observation of a fluorescent and a non-fluorescent bead as a function of diameter.

fluorescent photons compensate the micro-eclipse effect from a non-fluorescent bead. Fig. 4(b) shows the ratio between the normalized differential photon counts of fluorescently-labeled and non-fluorescent beads.

3.3. Beads and cells detection

Two different experiments were carried out in the proposed setup. We first tested the working principle of our system by evaluating the response of the device to both fluorescent and non-fluorescent magnetic beads of different diameters. 3 and 6 μm diameter non-fluorescent beads were introduced in the channel, and the output produced by the SPADs, when a single bead of each kind was present above it, was recorded. We then repeated the measurements for 3 μm diameter and 6 μm diameter fluorescent beads. Finally, a solution prepared by mixing equal concentrations (2×10^4 particles/mL) of fluorescent beads with non-fluorescent beads (10 μm diameter) was tested. The solution was injected in the channel and the flow was controlled using the external pump, as described in Section 3.1. Optical micrographs were taken when the flow was stopped (left panel of Fig. 5(a)) and compared with the fluorescent images obtained upon application of the fluorescent excitation source and filter set (right panel of Fig. 5(a)). These images allowed discriminating the presence of either fluorescent or non-fluorescent beads above a SPAD, and permitted direct comparison with the photon count measurements of the SPADs. Fig. 5(b) is a histogram representing the distribution of the SPAD differential photon counts upon the presence of either a fluorescent or a non-fluorescent bead. The differential photon count (x-axis) is discretized in intervals of 0.25%, while the y-axis shows the number of events per interval. We have cross-checked each SPAD measurement by separate optical observation through the microscope. In general, and according to the physical phenomena explained before, a lower differential photon count corresponds to the presence of a fluorescent bead, while a larger differential output corresponds to the presence of a non-fluorescent bead. The statistical fluctuation in the histogram distribution can have different origins: (i) fluctuations in size of the beads, (ii) differences in positioning over a SPAD, and (iii) in the case of fluorescent beads, fluctuations in the emitted fluorescence. Despite all these possible statistical variations, our system achieved a very good performance. Fig. 5(c) is a box plot of the differential photon count, showing that a difference between the two responses is large enough to accurately determine if a particle above a SPAD is fluorescent – or not. Indeed, 50% of the fluorescent beads contributed a differential photon count comprised in the 3.5–4.0% range, while 50% of the non-fluorescent particles were in the 6.8–7.5% interval.

Using the same operation conditions, a mixed solution of non-fluorescent Jurkat cells and immunofluorescent MCF-7 cells was prepared in a 4:6 ratio for studying the specificity of fluorescent detection, mimicking a realistic application of discriminating fluorescently-labeled cancer cells against a background of T lymphocytes. Similar to the experiments with beads, optical micrographs (left panel of Fig. 6(a)) were compared with fluorescent images (right panel of Fig. 6(a)) of the cells stopped in the channel to allow discriminating the presence of either fluorescent or non-fluorescent cells above a SPAD. Fig. 5(b) presents the results of cells detection. The histogram shows the distribution of the signals caused by the presence of either a fluorescent MCF-7 or a non-fluorescent Jurkat cell above the SPADs, cross-checked by separate optical control through the microscope. The presence of a MCF-7 cell causes a differential photon count of around 5.3% with respect to the reference signal, obtained in the absence of cells, while the presence of a non-fluorescent Jurkat cell causes a differential output in the range of 8.5%. The statistical variation of the results is larger than obtained for the beads, because of the larger fluctuations of

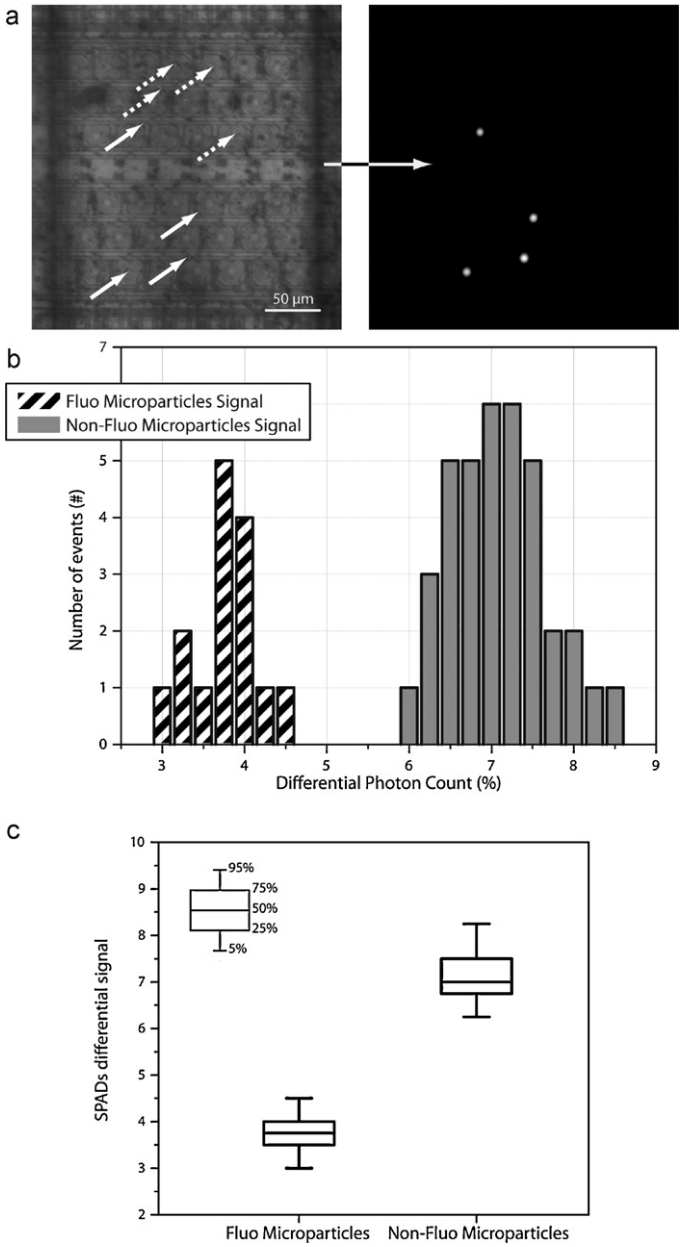

Fig. 5. Detection of beads in the microfluidic cartridge. (a) (left) Micrograph of fluorescent (full arrows) and non-fluorescent (dashed arrows) beads positioned over the SPAD matrix. (right) Using a fluorescent filter set on the microscope, only the fluorescently labeled beads are visible. (b) Distribution of fluorescent and non-fluorescent bead detection events. The differential photon count is derived from the photon count by subtraction and normalization with the SPADs photon count in the absence of the particle over the SPAD. (c) Box plot of fluorescent and non-fluorescent bead detection events, showing a clear discrimination of the differential photon count for fluorescent and non-fluorescent beads.

size and fluorescence of the cells. Fig. 6(c) clearly shows that our system is able to distinguish with a good precision a MCF-7 cell from a Jurkat cell. Of all the fluorescent MCF-7 cells detected, 50% was in the 4.8–5.5% range, and 90% was in the 4.0–7.0% range. Of all the non-fluorescent Jurkat cells, 50% was in the 8.0–9.0% range, and 90% in the 7.5–9.5% range. These results show that we are able to count the cells in the microfluidic channel with single cell resolution. While we have still cross-checked all SPADs measurements with microscope observation, our method in principle allows fluorescence detection without the use of a microscope and fluorescent detection filter. This proof of principle could be further exploited

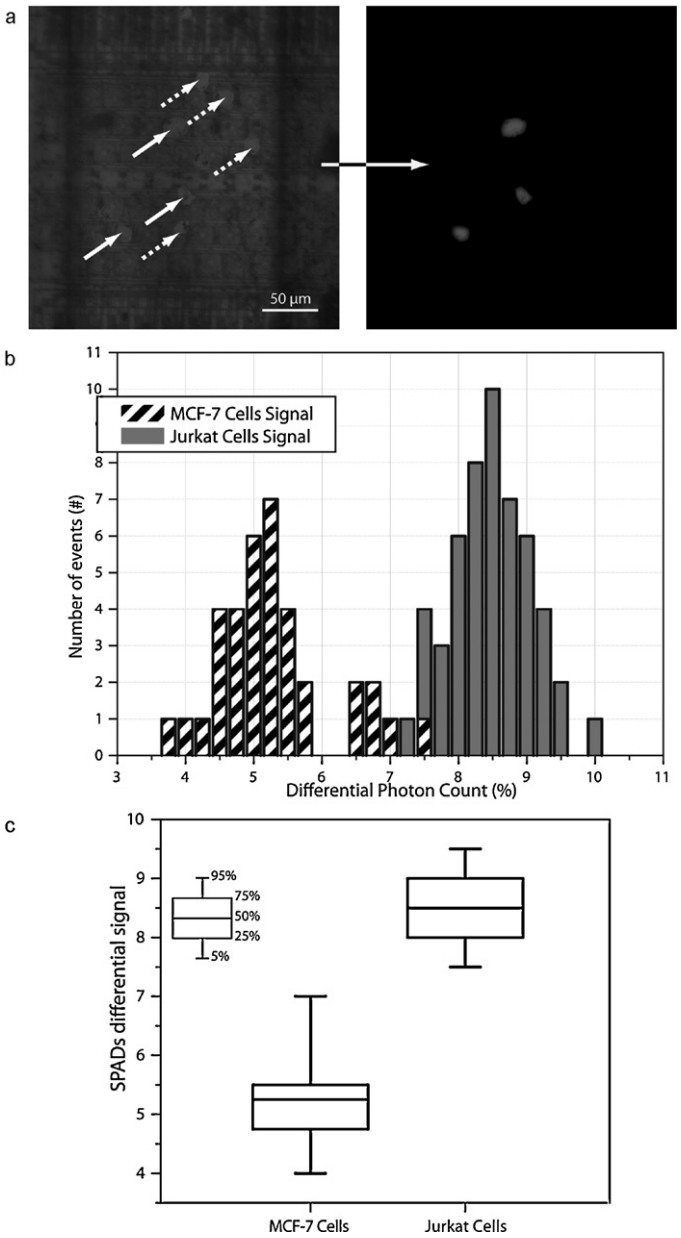

Fig. 6. Detection of single cells in the microfluidic cartridge. (a) (left) Micrograph of fluorescently labeled MCF-7 cells (full arrows) and non-fluorescent Jurkat cells (dashed arrows) positioned over the SPAD matrix. (right) Using a fluorescent filter set, only the fluorescently labeled MCF-7 cells are visible. (b) Distribution of fluorescent and non-fluorescent cell detection events. (c) Box plot of fluorescent MCF-7 and non-fluorescent Jurkat cell detection events.

in future, when designing a chip with a higher number of SPADs, allowing increased parallelization of the counting process.

4. Conclusions

We demonstrated the recognition of single fluorescently-labeled magnetic beads and cells in a test solution of mixed fluorescent and non-fluorescent elements, without the need of a bulky and expensive fluorescent microscope setup. Moreover, due to the use of a SPAD matrix spanning the complete width of the microchannel, our system does not require any particle focusing mechanism, needed when using a single detector. This allowed the use of a very simple, easily replicable and disposable microfluidic cartridge. Considering the dimensions of the current SPAD matrix and taking a unit time of the microfluidic stop and flow protocol of 3 s, our device would be able to perform around 1000 counting events per minute, when operated in a fully automated mode. Our system enables facile detection of particles and cells in a range of 3–10 μm, which is comparable to the performances of existing cell counting devices, allowing utilization for most biological applications. Our experiments indicate that the combination of advanced CMOS technology and microfluidics can result in a flexible and easy-to-use hybrid system for cell detection and discrimination, which holds large potential for future application in an analytical laboratory, at the point-of-care, or in a resource-limited environment.

References

[1] M.A.M. Gijs, F. Lacharme, U. Lehmann, Microfluidic applications of magnetic particles for biological analysis and catalysis, Chemical Reviews 110 (3) (2010) 1518–1563.
[2] M. Cristofanilli, G.T. Budd, M.J. Ellis, A. Stopeck, J. Matera, M.C. Miller, J.M. Reuben, G.V. Doyle, W.J. Allard, L.W.M.M. Terstappen, D.F. Hayes, Circulating tumor cells, disease progression, and survival in metastatic breast cancer, Seminars in Oncology 351 (8) (2004) 781–791.
[3] J.W. Mellors, A. Munoz, J.V. Giorgi, J.B. Margolick, C.J. Tassoni, P. Gupta, L.A. Kingsley, J.A. Todd, A.J. Saah, R. Detels, J.P. Phair, C.R. Rinaldo, Plasma viral load and CD4(+) lymphocytes as prognostic markers of HIV-1 infection, Annals of Internal Medicine 126 (12) (1997) 946–954.
[4] W.A. OBrien, P.M. Hartigan, E.S. Daar, M.S. Simberkoff, J.D. Hamilton, Changes in plasma HIV RNA levels and CD4(+) lymphocyte counts predict both response to antiretroviral therapy and therapeutic failure, Annals of Internal Medicine 126 (12) (1997) 939–945.
[5] W.A. OBrien, P.M. Hartigan, D. Martin, J. Esinhart, A. Hill, S. Benoit, M. Rubin, C. Lahart, N. Wray, S.M. Finegold, W.L. George, G.M. Dickinson, N. Klimas, G. Diamond, S.B. ZollaPazner, P.C. Jensen, C. Hawkes, C. Oster, F. Gordin, A.M. Labriola, P. Spivey, T. Matthews, K. Weinhold, G. Drusano, M.J. Egorin, Changes in plasma HIV-1 RNA and CD4+ lymphocyte counts and the risk of progression to AIDS, New England Journal of Medicine 334 (7) (1996) 426–431.
[6] WHO, 4 November, 2005. World Health Organization Patient Monitoring Guidelines for HIV Care and ART.
[7] W.A. Bonner, R.G. Sweet, H.R. Hulett, Herzenbe La, Fluorescence activated cell sorting, Review of Scientific Instruments 43 (3) (1972), 404-&.
[8] L. Kim, Y.-C. Toh, J. Voldman, H. Yu, A practical guide to microfluidic perfusion culture of adherent mammalian cells, Lab Chip 7 (2007) 681–694.
[9] R. Manz, M. Assenmacher, E. Pflüger, S. Miltenyi, A. Radbruch, Analysis and sorting of live cells according to secreted molecules, relocated to a cell-surface affinity matrix, Proceedings of the National Academy of Sciences of the United States of America 92 (6) (1995) 1921–1925.
[10] J.M. Kruger, T. Fukushima, V. Cherepanov, N. Borregaard, C. Loeve, C. Shek, K. Sharma, A.K. Tanswell, C.W. Chow, G.P. Downey, Protein–tyrosine phosphatase MEG2 is expressed by human neutrophils – localization to the phagosome and activation by polyphosphoinositides, Journal of Biological Chemistry 277 (4) (2002) 2620–2628.
[11] I. Schmid, C.H. Uittenbogaart, J.V. Giorgi, Sensitive method for measuring apoptosis and cell-surface phenotype in human thymocytes by flow-cytometry, Cytometry 15 (1) (1994) 12–20.
[12] P.A. Auroux, D. Iossifidis, D.R. Reyes, A. Manz, Micro total analysis systems. 2. Analytical standard operations and applications, Analytical Chemistry 74 (12) (2002) 2637–2652.
[13] A. Van Den Berg, T.S.J. Lammerink, in: A. Manz, H. Becker (Eds.), Microsystem Technology in Chemistry and Life Science, Springer, Berlin, 1998, pp. 21–49.
[14] T. Vilkner, D. Janasek, A. Manz, Micro total analysis systems, recent developments, Analytical Chemistry 76 (12) (2004) 3373–3385.
[15] J. West, M. Becker, S. Tombrink, A. Manz, Micro total analysis systems: latest achievements, Analytical Chemistry 80 (12) (2008) 4403–4419.
[16] P. Yager, T. Edwards, E. Fu, K. Helton, K. Nelson, M.R. Tam, B.H. Weigl, Microfluidic diagnostic technologies for global public health, Nature (2006) 442.
[17] H.A. Andersson, A. Van Den Berg (Eds.), Lab-on-Chips for Cellomics, Kluwer Academic Publishers, Dordrecht, 2004.
[18] J. El-Ali, P.K. Sorger, K.F. Jensen, Cells on chips, Nature 442 (2006) 403–411.
[19] A.Y. Fu, H.P. Chou, C. Spence, F.H. Arnold, S.R. Quake, An integrated microfabricated cell sorter, Analytical Chemistry 74 (11) (2002) 2451–2457.
[20] J.V. Jokerst, P.N. Floriano, N. Christodoulides, G.W. Simmons, J.T. McDevitt, Integration of semiconductor quantum dots into nano-bio-chip systems for enumeration of CD4+ T cell counts at the point-of-need, Lab on a Chip – Miniaturisation for Chemistry and Biology 8 (12) (2008) 2079–2090.
[21] X. Cheng, D. Irimia, M. Dixon, K. Sekine, U. Demirci, L. Zamir, R.G. Tompkins, W. Rodriguez, M. Toner, A microfluidic device for practical label-free CD4+ T cell counting of HIV-infected subjects 7 (2) (2007) 170–178.
[22] X.Q. Jiang, M.G. Spencer, Electrochemical impedance biosensor with electrode pixels for precise counting of CD4(+) cells: a microchip for quantitative diagnosis of HIV infection status of AIDS patients, Biosensors and Bioelectronics 25 (7) (2010) 1622–1628.
[23] O. Mudanyali, C. Oztoprak, D. Tseng, A. Erlinger, A. Ozcan, Detection of waterborne parasites using field-portable and cost-effective lensfree microscopy, Lab on a Chip 10 (18) (2010) 2419–2423.

[24] O. Mudanyali, D. Tseng, C. Oh, S.O. Isikman, I. Sencan, W. Bishara, C. Oztoprak, S.K. Seo, B. Khademhosseini, A. Ozcan, Compact, light-weight and cost-effective microscope based on lensless incoherent holography for telemedicine applications, Lab on a Chip 10 (11) (2010) 1417–1428.
[25] D. Tseng, O. Mudanyali, C. Oztoprak, S.O. Isikman, I. Sencan, O. Yaglidere, A. Ozcan, Lensfree microscopy on a cellphone, Lab on a Chip 10 (14) (2010) 1787–1792.
[26] A.F. Coskun, I. Sencan, T.W. Su, A. Ozcan, Lensless wide-field fluorescent imaging on a chip using compressive decoding of sparse objects, Optics Express 18 (10) (2010) 10510–10523.
[27] A.F. Coskun, T.W. Su, A. Ozcan, Wide field-of-view lens-free fluorescent imaging on a chip, Lab on a Chip 10 (7) (2010) 824–827.
[28] C. Niclass, A. Rochas, P.A. Besse, E. Charbon, Design and characterization of a CMOS 3-D image sensor based on single photon avalanche diodes, IEEE Journal of Solid-State Circuits 40 (9) (2005) 1847–1854.
[29] U. Lehmann, M. Sergio, S. Pietrocola, E. Dupont, C. Niclass, M.A.M. Gijs, E. Charbon, Microparticle photometry in a CMOS microsystem combining magnetic actuation and in situ optical detection, Sensors and Actuators B: Chemical 132 (2) (2008) 411–417.
[30] P. Sartoretti, J. Schneider, On the detection of satellites of extrasolar planets with the method of transits, Astronomy and Astrophysics Supplement Series 134 (3) (1999) 553–560.
[36] R.J. Fulton, R.L. McDade, P.L. Smith, L.J. Kienker, J.R. Kettman, Advanced multiplexed analysis with the FlowMetrix(TM) system, Clinical Chemistry 43 (9) (1997) 1749–1756.
[39] K.W. Kwon, S.S. Choi, H.S. Lee, B. Kim, S.N. Lee, M.C. Park, P. Kim, S.Y. Hwang, K.Y. Suh, Label-free, microfluidic separation and enrichment of human breast cancer cells by adhesion difference, Lab Chip 7 (2007) 1461–1468.
[40] A. Landay, B. Ohlssonwilhelm, J.V. Giorgi, Application of flow-cytometry to the study of HIV-infection, Aids 4 (6) (1990) 479–497.
[43] M.A. McClain, C.T. Culbertson, S.C. Jacobson, N.L. Albritton, C.E. Sims, J.M. Ramsey, Microfluidic devices for the highthroughput chemical analysis of cells, Analytical Chemistry 75 (2003) 5646–5655.
[45] P. Nath, J. Strelnik, A. Vasanji, L.R. Moore, P.S. Williams, M. Zborowski, S. Roy, A.J. Fleischman, Development of multistage magnetic deposition microscopy, Analytical Chemistry 81 (2009) 43–49.
[49] D.A.A. Vignali, Multiplexed particle-based flow cytometric assays, Journal of Immunological Methods 243 (1-2) (2000) 243–255.
[50] M.M. Wang, E. Tu, D.E. Raymond, J.M. Yang, H.C. Zhang, N. Hagen, B. Dees, E.M. Mercer, A.H. Forster, I. Kariv, P.J. Marchand, W.F. Butler, Microfluidic sorting of mammalian cells by optical force switching, Nature Biotechnology 23 (2005) 83–87.

Biographies

Emile P. Dupont received the Laurea *cum laude* from the Politecnico di Torino in 2004, the M.S. degree from EPFL, Politecnico di Torino, and INPG in 2006, and the Ph.D. degree from EPFL in 2010 all in Electrical Engineering. In 2005 he was a visiting student in EE at Cambridge Univ. and in 2006 he was visiting technical student at CERN in Geneva.

Estelle Labonne was born in 1980. She received the B.S. degree from the University of Montpellier in 2001, the M.S. and the Ph.D. degrees from the Grenoble Polytechnic National Institute in 2002 and 2006, respectively. She has collaborated with STMicroelectronics, TMI-ORION, and Wrexham University.

Yuki Maruyama received the B.S., the M.S., and the Ph.D. degrees in Electrical Engineering from Toyohashi University of Technology in 2003, 2005, and 2008, respectively. He has since been a post-doctoral fellow at EPFL and TU Delft. He has published over 20 articles in peer-reviewed journals and proceedings, and he holds 2 patents. In 2004 Dr. Maruyama has received the Outstanding Student Performance Award from the Institute of Image Information and Television Engineers.

Caroline Vandevyver received her degree in biochemistry in 1985 from the Katholieke Universiteit Leuven, Belgium and her Ph.D. degree in biotechnology at the same university in 1989. She joined the Biomedical Research Institute "Dr. L- Willems Instituut" in Hasselt, Belgium, in 1989. Subsequently, she has worked there on T cell mediated autoimmune diseases (Multiple Sclerosis, Rheumatoid Arthritis), genetic association and linkage studies in multifactorial diseases, mutation analysis of genetic disorders (Phenylketonuria, alpha 1 anti-trypsine deficiency, congenital adrenal hyperplasia) and the development of active and passive immune therapies for cancer. She joined EPFL in 2000 at the Laboratory of Chemical Biotechnology headed by Prof. Ruth Freitag, where she was responsible for the cell culture lab and the (recombinant) protein purification and characterization. She joined the Laboratory of Lanthanide Supramolecular Chemistry (LCSL) in May 2006, where she is responsible for the live cell imaging project with Lanthanide complexes.

Ulrike Lehmann was born in Rostock, Germany in 1978. She obtained her Dipl-Ing. degree in electrical engineering, with a specialization on MEMS, in 2003 at the Chemnitz Technical University, Chemnitz, Germany. She is currently following her doctoral studies at the Ecole Polytechnique Fédérale de Lausanne (EPFL) in the Laboratory for Microsystems. Her Ph.D. work encompasses the manipulation of magnetic microparticles for application in biomedical systems.

Martin A.M. Gijs received his degree in physics in 1981 from the Katholieke Universiteit Leuven, Belgium and his Ph.D. degree in physics at the same university in 1986. He joined the Philips Research Laboratories in Eindhoven, The Netherlands, in 1987. Subsequently, he has worked there on micro-and nano-fabrication processes of high critical temperature superconducting Josephson and tunnel junctions, the microfabrication of microstructures in magnetic multilayers showing the giant magnetoresistance effect, the design and realization of miniaturized motors for hard disk applications and the design and realization of planar transformers for miniaturized power applications. He joined EPFL in 1997. His present interests are in developing technologies for novel magnetic devices, new microfabrication technologies for microsystems fabrication in general and the development and use of microsystems technologies for microfluidic and biomedical applications in particular.

Edoardo Charbon (SM'00) received the Diploma from ETH Zurich in 1988, the M.S. degree from UCSD in 1991, and the Ph.D. degree from UC-Berkeley in 1995, all in Electrical Engineering and EECS. From 1995 to 2000, he was with Cadence Design Systems, where he was the architect of the company's initiative on information hiding for intellectual property protection. In 2000, he joined Canesta Inc. as its Chief Architect, leading the development of wireless 3-D CMOS image sensors. Since November 2002, he has been a member of the Faculty of EPFL in Lausanne, Switzerland, working in the field of CMOS sensors, bio-photonics, and ultra low-power wireless embedded systems. In Fall 2008 he has joined the Faculty of TU Delft, as full professor in VLSI design, succeeding Patrick Dewilde. Dr. Charbon has consulted for numerous organizations, including Bosch, Texas Instruments, Agilent, and the Carlyle Group. He has published over 200 articles in technical journals, conference proceedings, magazines, and two books; he holds 13 patents. His research interests include 3D imaging, advanced bio- and medical imaging, quantum integrated circuits, and space-based detection.